SUPPORTING INFORMATION APPENDIX

MINFLUX monitors rapid molecular jumps with superior spatiotemporal resolution

Yvan Eilers[a,†], Haisen Ta[a,†], Klaus C. Gwosch[a], Francisco Balzarotti[a], and Stefan W. Hell[a,b*]

[a]Department of NanoBiophotonics, Max Planck Institute for Biophysical Chemistry, Am Faßberg 11, 37077 Göttingen, Germany

[b]Department of Optical Nanoscopy, Max Planck Institute for Medical Research, Jahnstr. 29, 69120 Heidelberg, Germany

† The authors contributed equally to this work.

* Corresponding author: shell@mpibpc.mpg.de

www.pnas.org/cgi/doi/10.1073/pnas.1801672115

CONTENTS

LIST OF SUPPLEMENTARY FIGURES

Materials and Methods

Sample preparation

DNA origami sample preparation

Fig. 2A shows a cartoon of a fluorescent emitter (ATTO 647N) attached to a 30 nucleotide (nt) single stranded DNA (ssDNA). It was complimentarily paired to a second ssDNA with a 33 nt base pairing on a rectangular DNA origami. The ATTO 647N molecule was close to the DNA origami base by design. The rectangular DNA origami was a modified Rothemund rectangular origami (1) with 5 biotinylated staple sequences for fixation on the coverslip via streptavidin-biotin linkage, and a double stranded DNA strand sticking out of the DNA origami plane with an ATTO 647N emitter. Fig. 3A shows a cartoon of the designed 1D diffuser. In this case, two extended staple strands were base paired with one DNA bridge strand. An ATTO 647N emitter was attached approximately at the center of the bridge with a maximal distance of about 10 nm from the origami base. The two arms of the bridge were much shorter than the persistence length of dsDNA (2, 3) and should therefore maintain a triangle conformation, allowing the emitter to move on a half circle above the origami thus restricting it to a one-dimensional movement.

DNA origami assembly

The origami strands were annealed into a DNA origami using a folding buffer consisting of $1 \times TAE$ (40 mM Tris, 20 mM Accetate and 1 mM EDTA, Sigma-Aldrich) with 12.5 mM $MgCl_2$ (Magnesium chloride hexahydrate $M2670$, Sigma-Aldrich) $\mathrm{pH} = 8$. The sequences for the DNA strands are provided in the SI Appendix (Staples and DNA strand sequences). Note that the staples need to be combined following the stated order. Strands with the numbers $11, 28, 123, 191$ and 208 were biotinylated with biotin modification at the $5'$ end. Including the unmodified, biotinylated and modified helping staples, the final solution contained 200 nM staples and 20 nM scaffold. Staple number 76 was substituted by a 63 nucleotides ssDNA (76 single molecule helper) to obtain the ssDNA solution. Staple 22 and 76 were exchanged to Nes22 (1DD 22) and Nes76 (1DD 76) helper ssDNA in the origami annealing pool to obtain the 1DD bridge solution.

The ssDNA solution as well as the 1DD bridge solution were thermally annealed by heating to 85°C for 3 min, cooled to 42°C at 0.5°C/min and then rapidly cooled to 4°C using a thermocycler (TPersonal, Biometra GmbH). Subsequently, the DNA origami were purified. The solution was mixed $(1{:}\,1)$ with a PEG buffer (15 % PEG (Poly(ethylene glycol), BioUltra, molecular weight 8000, Sigma-Aldrich), 500 mM $NaCl$ (Sodium chloride, ≥ 99 %, Sigma-Aldrich) and 12.5 mM $MgCl_2$ (Magnesium Chloride hexahydrate, M2670, Sigma-Aldrich). The resulting solution was centrifuged at 20000 rcf for 30 min. The supernatant was discarded and the precipitate resuspended in folding buffer by vortexing. The purification procedure was performed three times. This procedure results in either ssDNA origami or 1DD origami.

Immobilizing the origami

Flow channels as well as cleaned cover slips were obtained as described previously (4). The flow channel was filled with 20 µl of 2 mg/ml biotinylated BSA solution dissolved in PBS for 5-10 min and washed with PBS. Subsequently, 40 µl of 0.5 mg/ml streptavidin solution dissolved in PBS was added for 5 min. After washing with folding buffer, 30 µl of DNA origami (100 pM of either ssDNA origami or 1DD origami) were added and thus immobilized on the coverslip. Then, 30 µl (~ 200 pM) of the single molecule strand (SM strand) or alternatively of the bridge (1DD bridge) was added. The density of the DNA origami was $< 0.1/\mu\mathrm{m}^2$. ROXS buffer (5) was added before the sample was sealed with epoxy glue (Loctite EA 3430, Henkel) for final imaging. AFM measurements (Asylum research MFP 3D, Oxford Instruments Asylum Research, Inc.) assured that the origami indeed folded adequately (see Fig. **S1**).

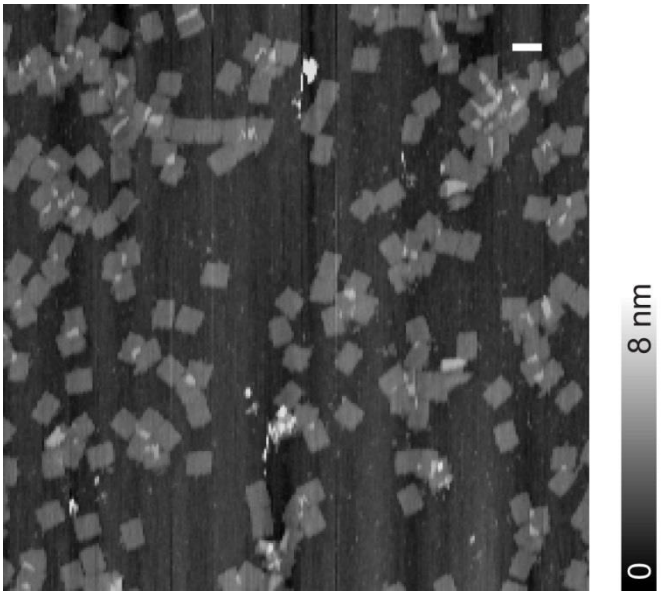

Fig. S1. AFM images of DNA origami. The DNA origamis were immobilized on a glass surface via biotin-streptavidin linkage. The glass surface was coated by biotinylated bovine serum albumin (BSA). The cantilever was in tapping mode. The grey scale codes the height. Scan area, 2×2um^2; scale bar, 100 nm.

Experimental setup

The utilized optical setup (fig. **S2A**) closely followed the previously reported design (4). Excitation light with a wavelength of 642 nm is delivered by Laser 1 (VFL-P-1500-642, MPB Communications Inc.) with its power controlled by an acoustio-optic tunable filter (AOTF) (AOTFnC VIS, AA Sa). An electro-optical modulator (EOM) (LM 0202 P 5W & LIV 20, Qioptiq Photonics GmbH & Co. KG) enabled fast amplitude modulation. A 2π vortex phase plate (VPP) (VPP-1a, RPC Photonics) modulated the wavefront of the excitation beam so that it rendered a doughnut-shaped spot of excitation light in the focal plane of the oil immersion objective lens (HCX PL APO 100x/1.40-0.70 Oil CS, Leica Microsystems GmbH). Laser 2 emitting at 640 nm (LDH-D-C-640, PicoQuant) was employed for widefield illumination.

Two orthogonal non-descanned electro-optical deflectors (EODx and EODy) (M-311-A, Conoptics Inc.) were used for fast lateral scanning of the excitation beam. The deflectors were driven by two high voltage amplifiers in a differential arrangement (PZD700A, Trek Inc., Lockport, NY, USA & WMA-300 Falco Systems BV). The fast amplifier provided a bandwidth of 5 MHz and a scanning range of ± 300 nm. It was employed for fast beam multiplexing in order to generate the time shifted STC (see fig. **S2B**). The second amplifier with a bandwidth of 125 kHz and a field of view of ± 1 µm was mainly used for PSF measurements. Initial superposition of the center of the STC with the target emitter of interest was achieved by a descanned tip/tilt mirror (PSH-$10/2$ & EVD300, both Piezosysteme Jena GmbH) with 1 kHz bandwidth and a 20×30 µm scan range. A field programmable gate array board (FPGA) (NI PCIe-7852R, National Instruments) controlled all scanners.

The emitter fluorescence was collected in back-scattering geometry. A dichroic mirror DM1 (Z$488/633$RDC, Chroma Technology Corp.) separated the fluorescence from the excitation light. The fluorescence was spectrally filtered by F1 (FF01-635/LP-25 & FF01-842/SP-25, Semrock Inc.) or F2 (ET$700/75$m & ZET642NF, Chroma Technology Corp. & FF01-775/SP-25, Semrock Inc.) and imaged by Camera 1 (Luca S, Andor Technology Ltd.) or detected by the fiber coupled APD 1 (SPCM-AQRH-13-FC, Excelitas Technologies) with an approximately 400 nm field of view in the sample plane.

The sample was mounted on a piezoelectric stage (P-733.3-DD & E725, both Physik Instrumente GmbH & Co. KG) which allowed accurate positioning in three dimensions. A stage lock actively

stabilized the stage position in three dimensions. The design of this stabilization system (employing Laser 3, Camera 2 and 3) was previously published (4). Custom programs written in LabView (National Instruments) controlled the devices directly via the data acquisition (DAQ) boards (NI PCIe-6353 & NI PCI-6259, both National Instruments & USB-3103, Measurement Computing Corporation) or the FPGA board. To obtain photon arrival time traces, the fluorescence signal was split using a 50: 50 beam splitter prior to detection with two separate APDs (not shown in fig. **S2**, since this was used only for assessing the blinking dynamics, but not for the tracking experiment). A PicoHarp 300 module (PicoQuant) measured the precise photon arrival times.

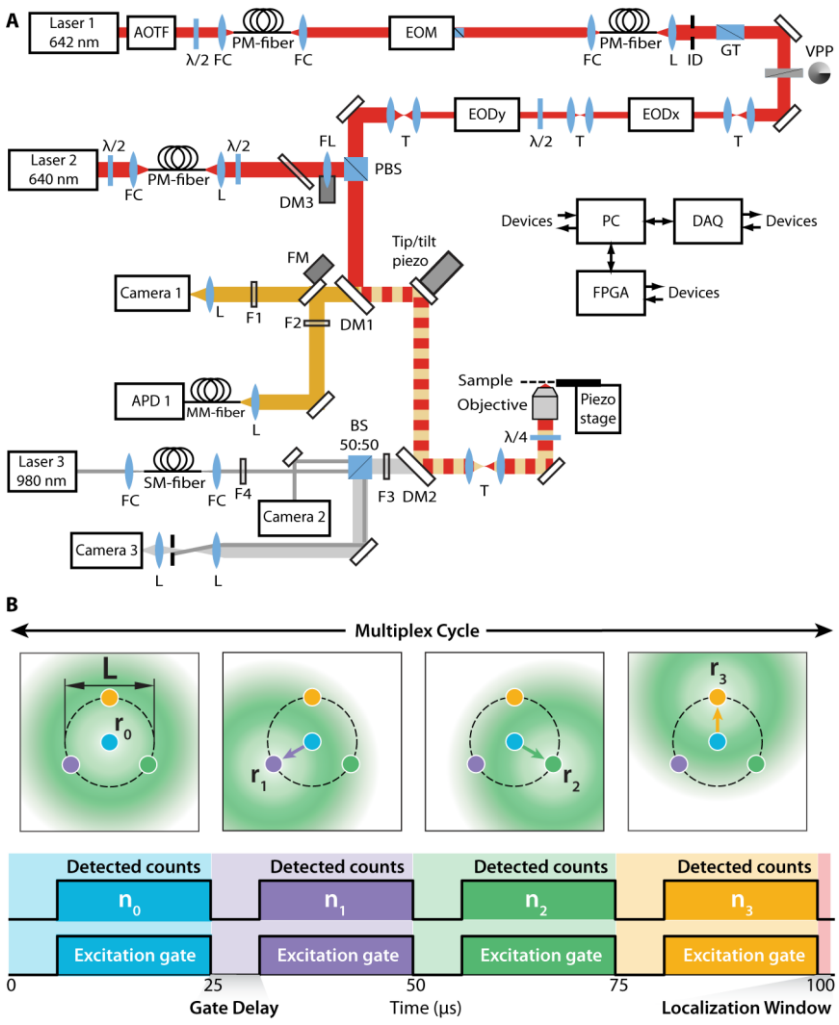

Fig. S2. Experimental setup and the set of targeted coordinates of the doughnut shaped excitation beam. (**A**) Schematic of the setup. $\lambda/2$: half wave plate (B. Halle Nachfl. GmbH), FC: fiber collimator 60FC (Schäfter + Kirchhoff), PM-fiber: polarization maintaining fiber (Thorlabs Inc. or Schäfter + Kirchhoff) SM-fiber: single mode fiber (Thorlabs Inc.), MM-fiber: multimode fiber (M31L01, Thorlabs Inc.), PBS: polarizing beam splitter cube (B. Halle Nachfl. GmbH), GT: Glan-Thompson prism (B. Halle Nachfl. GmbH), BS: beam splitter cube 50: 50 (B. Halle Nachfl. GmbH), L: achromatic lens with VIS or NIR AR coating (Thorlabs Inc. or Qioptiq Photonics GmbH & Co. KG), T: telescope, FL: lens on flip mount, FM : mirror on motorized flip mount, ID: iris diaphragm, PC: personal computer running Windows 7 (Microsoft Corp.) and LabView 2016 (National Instruments). The other elements are described in the text. (**B**) The set of targeted coordinates (STC) comprises a central point and three points that are equally distributed on a circle of diameter L. These points are sequentially addressed. The excitation intensity is modulated by the EOM. The off-time is given by the gate delay. After the four successive exposures (one STC cycle), a live position estimation can be calculated during the localization window employing the FPGA board.

Data acquisition

Prior to imaging, the stage was locked. Lateral position stabilization was achieved by locking to a Au nanorod in the field of view of camera 3 (SI Appendix, Experimental setup). To initialize a MINFLUX measurement, the STC has to be superimposed on the structure that is to be studied. To that end, we recorded a faint widefield image with approximately diffraction-limited spots of the emitters with camera 1 and selected the emitters of interest manually. Fitting a 2D Gaussian to the measured intensity profile yielded a coarse position estimation of the selected emitter. The excitation doughnut was directed to the retrieved coordinate by commanding the tip/tilt mirror. In order to optimize the centering of the STC on the emitter we employed a tracking routine. A proportional integral (PI) controller feedback routine optimized the superposition by commanding the tip/tilt mirror iteratively. The proportional and integral parameters of the controller were $p_k = 0$ and $p_i = 0.0087$. Live MINFLUX position estimation used the mLMS estimator that was described in detail previously (4). mLMS parameters were set to $k_i = 1.2$ and $\beta_1 = 3$. For this routine, the beam separation L was set to values in the range of $70 - 100$ nm. We used an excitation power of $10 - 200$ µW, measured close to the back focal plane of the objective. After about 500 ms, the feedback routine was turned off and the parameters adjusted for the tracking measurement.

We employed the STC visualized in fig. **S2**B. It consists of a multiplex cycle of four time-interleaved exposures to a displaced doughnut shaped beam $I_i(\bar{r}) = I(\bar{r} - \bar{r}_{bi})$ at positions

$$\bar{r}_{b0} = [0,0]^{\mathrm{T}}, \qquad \bar{r}_{bi} = \frac{L}{2}[\cos(\alpha_i), \sin(\alpha_i)], \qquad \text{for } \alpha_i = -\frac{2\pi}{3}\left(i + \frac{1}{4}\right) \; \forall \; i \in [1,3] \quad \text{(S1)}$$

This equals a central exposure followed by three peripheral exposures that reside on a circle of diameter L. The multiplex cycle rate was $\gamma_c = 10$ kHz and the detection and excitation gate were typically 17 µs with a gate delay of 7 µs. The beam separation was set to $L = 50$ nm and the excitation power increased by a factor of $5 - 10$. The count traces for the now stationary STC were collected as were background counts once the emitter was bleached. Subsequently, we recorded the next emitter of interest.

Data analysis

In order to obtain localizations from the measured count traces a couple of analysis steps were necessary as described below.

Segmentation and binning of the count traces

The fluorescence emission signal from the emitter had to be isolated from the initial centering routine as well as from the background contributions, once the emitter bleached. We segmented the trace in these three parts manually. The average background level λ_{bg} was estimated from the isolated background contributions and allowed the estimation of the signal to background ratio (SBR) for each multiplex cycle. The SBR is estimated by

$$SBR_j = \frac{N_j}{\lambda_{bg}} - 1 \qquad \text{(S2)}$$

where $N_j = \sum_{i=0}^{3} n_{ij}$ is the total number of detected photons during the jth multiplex cycle. Here, n_{ij} is the number of photons collected for exposure i in multiplex cycle j. In this study we measured typical SBR values of $\langle SBR \rangle = 12.5 \pm 4$ using $L = 50$ nm.

The multiplex cycle rate was set to $\gamma_c = 10$ kHz. This enabled time resolutions of 100 µs per localization. Given the $1/\sqrt{N}$ dependence of the localization precision, the spatial precision can be increased upon reduction of the temporal resolution by binning the counts. To that end, the counts

n_{ij} of the ith exposure of the jth multiplex cycle are added to counts of the ith exposure of subsequent multiplex cycles. For a b-fold binning, b count values were added in a channel, respectively

$$\mathrm{n}_{\mathrm{ik}}^{(\mathrm{b})} = \sum_{j=(k-1)b+1}^{k\cdot b} n_{ij} \tag{S3}$$

The binned counts $\left[\mathrm{n}_{0\mathrm{k}}^{(\mathrm{b})}, \dots, \mathrm{n}_{3\mathrm{k}}^{(\mathrm{b})}\right]$ of the four channels are used for localization. The total number of counts per localization after binning is thus given by $N_j^{(b)} = \sum_{i=0}^{3} n_{ij}^{(b)}$.

Localization

Localizing an emitter using MINFLUX entails knowing the excitation profile $I(\bar{r})$ and its spatial placement in order to localize the emitter at $\bar{r}_m \in \mathbb{R}^2$ given the measured counts $\bar{n} = [n_0, \dots, n_3]$. A detailed derivation of the underlying theory was published recently (4).

Localization precision

In this study, the localization precision σ is defined as the arithmetic mean of the eigenvalues of the covariance matrix Σ

$$\sigma(\bar{r}) = \sqrt{\frac{1}{2}\mathrm{tr}\big(\Sigma(\bar{\mathrm{r}})\big)} \tag{S4}$$

where $\mathrm{tr}(\Sigma)$ is the trace of the covariance matrix.

We further define the isotropy ב as

$$\text{ב}(\bar{r}) = \sqrt{\frac{\min\limits_{\mathrm{i}\in[1,2]} \sigma_i(\bar{r})}{\max\limits_{\mathrm{i}\in[1,2]} \sigma_i(\bar{r})}} \tag{S5}$$

Where σ_i are the eigenvalues of the covariance matrix Σ.

Autocorrelation analysis

This section explains how we obtained the magnitude of the emitter movement σ_{mov} from a MINFLUX localization trace $\{\hat{\bar{r}}\} = \{\hat{\bar{r}}_1, \dots, \hat{\bar{r}}_M\}$ containing M localizations. Note that the covariance matrix $\boldsymbol{\Sigma}$ of this trace contains contributions from the localization uncertainty as well as from a possible emitter movement $\{\bar{r}_{mov}\}$. The covariance matrix $\boldsymbol{\Sigma}$ of a two dimensional localization trace $\{\hat{\bar{r}}\}$ can be expressed in terms of its correlation $\boldsymbol{R}$:

$$\Sigma_{ij} = \frac{M}{M-1} R_{ij}\big(0, \{\hat{\bar{r}}\}\big) \tag{S6}$$

$$R_{ij}\big(m, \{\hat{\bar{r}}\}\big) = \frac{1}{M-m} \sum_{k=1}^{M-m} \big(\hat{r}_{i,k+m} - \langle \hat{r}_i \rangle\big)\big(\hat{r}_{j,k} - \langle \hat{r}_j \rangle\big) \tag{S7}$$

with M being the number of localizations in $\{\hat{\bar{r}}\}$. The symbol $\hat{r}_{i,k}$ represents the component i ($i \in [1,2]$ for a 2D localization) of the trajectory at time sample k ($k \in [1, \dots, M]$), while $\langle \hat{r}_i \rangle$ is the time-averaged component i. Given that localization uncertainty noise is uncorrelated, the correlation of $\{\hat{\bar{r}}\}$ for lags larger than zero does not contain contributions from it, but information about the correlation of the movement only. To obtain an estimate of the covariance of the movement $\boldsymbol{\Sigma}^{\mathrm{mov}}$, we estimated $R_{ij}^{mov}(0, \{\hat{\bar{r}}\})$ from a spline fit to $R_{ij}(m, \{\hat{\bar{r}}\})$ for $m > 0$. The corresponding covariance of the movement $\boldsymbol{\Sigma}^{\mathrm{mov}}$ can then be obtained using eq. (S6).

Given that ideally we have a 1D movement (fig. **3A**) we rotated the 2D coordinate system such that one axis coincides with the direction of predominant emitter movement. Thereby, the eigenvectors $\bar{e}_1$ and $\bar{e}_2$, that point in the directions of the new axes, were obtained by calculating the normalized eigenvectors of the correlation matrix $R_{xy}(1, \{\hat{\bar{r}}\})$ with

$$R_{xy}\left(m, \{\hat{\bar{r}}\}\right) = \frac{1}{M-m} \sum_{k=1}^{M-m} (\hat{x}_{k+m} - \langle \hat{x} \rangle)(\hat{y}_k - \langle \hat{y} \rangle) \tag{S8}$$

The estimated magnitude of the movement $\hat{\sigma}_{mov,ii}$ is then defined by $\hat{\sigma}_{mov,ii} \equiv \sqrt{\Sigma_{ii}^{\mathrm{mov}}}$.

An example of this procedure is shown in fig. **S3**. We simulated 1D diffusive movement on a semicircle with a radius of 10 nm as given by the sample design (fig. **S3**A). Thereby, the origami surface was assumed to act as a reflective border. The diffusion coefficient was set to $D = 2500\ \mathrm{nm}^2/\mathrm{s}$ with a sampling time of 400 µs and $M = 12500$. Figure **S3**A1 shows the projection of this movement on the xy plane and fig. **S3**B shows a 300 ms extract of the corresponding x and y coordinates. For each emitter position, multinomial photon realizations were obtained using eq. (S1), where the total photons per realization were set to $N = 100$. The signal-to-background ratio was $\mathrm{SBR} = 10$ and the intensity profile $I(\bar{r})$ of the excitation beam assumed to be doughnut shaped as given by eq. (S13). Fig. **S3**C and **S3**A2 show the photon count realizations and the corresponding MINFLUX localizations (using the numLMS estimator). Figure **S3**A3 visualizes the localization histogram in the rotated coordinate system and fig. **S3**D shows the autocorrelation $R_{11}(m, \{\hat{\bar{r}}\})$ and $R_{22}(m, \{\hat{\bar{r}}\})$. Note that $R_{22}(m, \{\hat{\bar{r}}\})$ coincides very well with the autocorrelation of the known 1D movement R_{mov}^{1D}. To fit a spline to $R_{ii}(m > 0, \{\hat{\bar{r}}\})$ we used the function "fit" from the curve fitting toolbox in MATLAB. The library model used was "smoothingspline" with parameter "smoothingParam $= 0.99$". From the fit, the autocorrelation of the movement $R_{ii}^{mov}(0, \{\hat{\bar{r}}\})$ can be estimated and allows the estimation of $\hat{\sigma}_{mov,ii} = \sqrt{\Sigma_{ii}^{\mathrm{mov}}}$ using eq. (S6). In this case, the estimated magnitude is $\hat{\sigma}_{mov,11} = 7.02$ nm given an actual movement of $\sigma_{mov} = 7.08$ nm.

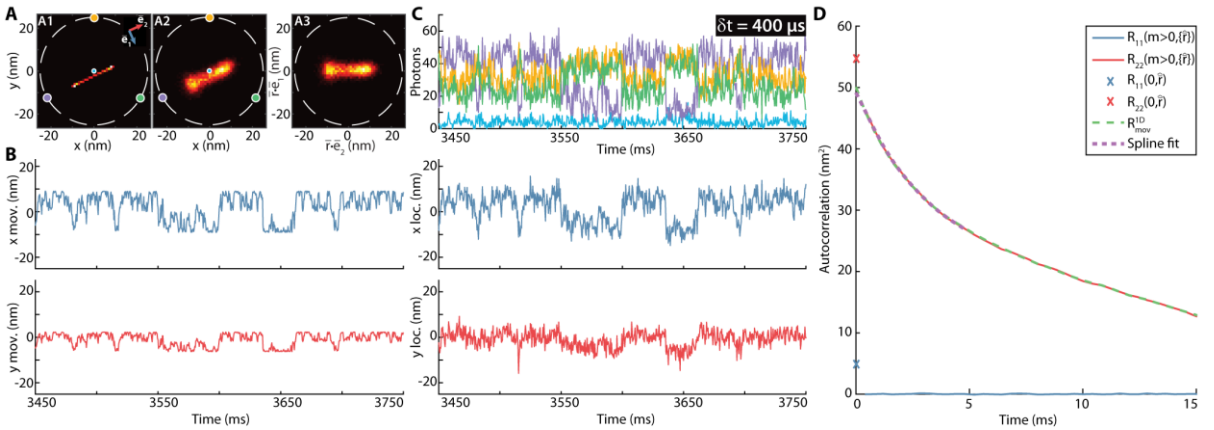

Fig. S3. Simulation of a 1D diffusive emitter movement on a half circle with a radius of 10 nm. (**A**) A1: histogram of a simulated trace $\{\bar{r}_{mov}\}$ of 5 s length with a time resolution of 400 µs. A2: histogram of the obtained MINFLUX localizations $\{\hat{\bar{r}}\}$ for $N = 100$ photons per localization and $L = 50$ nm. A3: histogram of the obtained localizations after a coordinate transformation: $\hat{\bar{r}} \cdot \bar{e}_2$ is the projection of $\hat{\bar{r}}$ on the direction of the emitter movement $(\bar{e}_2)$, $\hat{\bar{r}} \cdot \bar{e}_1$ the projection on $\bar{e}_1$ which is perpendicular to $\bar{e}_2$ (see text). (**B**) Time trace extract of the emitter movement $\{\bar{r}_{mov}\}$ used in A1. (**C**) Photon realizations for the trace extract shown in B and corresponding MINFLUX localizations $\{\hat{\bar{r}}\}$. (**D**) Autocorrelation of the MINFLUX localization trace $R_{11}(m, \{\hat{\bar{r}}\})$ and $R_{22}(m, \{\hat{\bar{r}}\})$. The autocorrelation of the simulated movement R_{mov}^{1D} as well as a spline fit to $R_{22}(m, \{\hat{\bar{r}}\})$ are overlaid. From this fit the standard deviation of the movement $\sigma_{mov,ii}$ along direction $\bar{e}_i$ can be estimated.

Trace classification

In this study a total of 496 traces belonging to different 1DD bridge origamis were evaluated. The mean trace length was 5.94 sec in these measurements, which corresponds to 14844 localizations at $\delta t = 400$ µs. To characterize the dynamics of the sample, the standard deviation σ_{mov} along the axis of maximal movement was calculated for each trace (see SI Appendix, Autocorrelation analysis). Evaluation of the occurrences of σ_{mov} reveals that the majority (> 50 %) of the 1DD bridge traces where actually standing still or moving only slightly (fig. **S4**). Only the minority (< 5 %) showed a one-dimensional movement with a peak-to-peak magnitude of about 20 nm as expected from sample design (see SI Appendix, DNA origami sample preparation). The remainder consists of traces with a one-dimensional movement having a reduced magnitude or traces that are rather immobile or that move randomly in a restricted area.

Figure **S4** also visualizes the localization histograms of some representative traces spanning the whole range of obtained σ_{mov} values. The detected photon counts and the respective MINFLUX localizations as well as the correlation analysis of these traces are shown in fig. **S5** and **S6**.

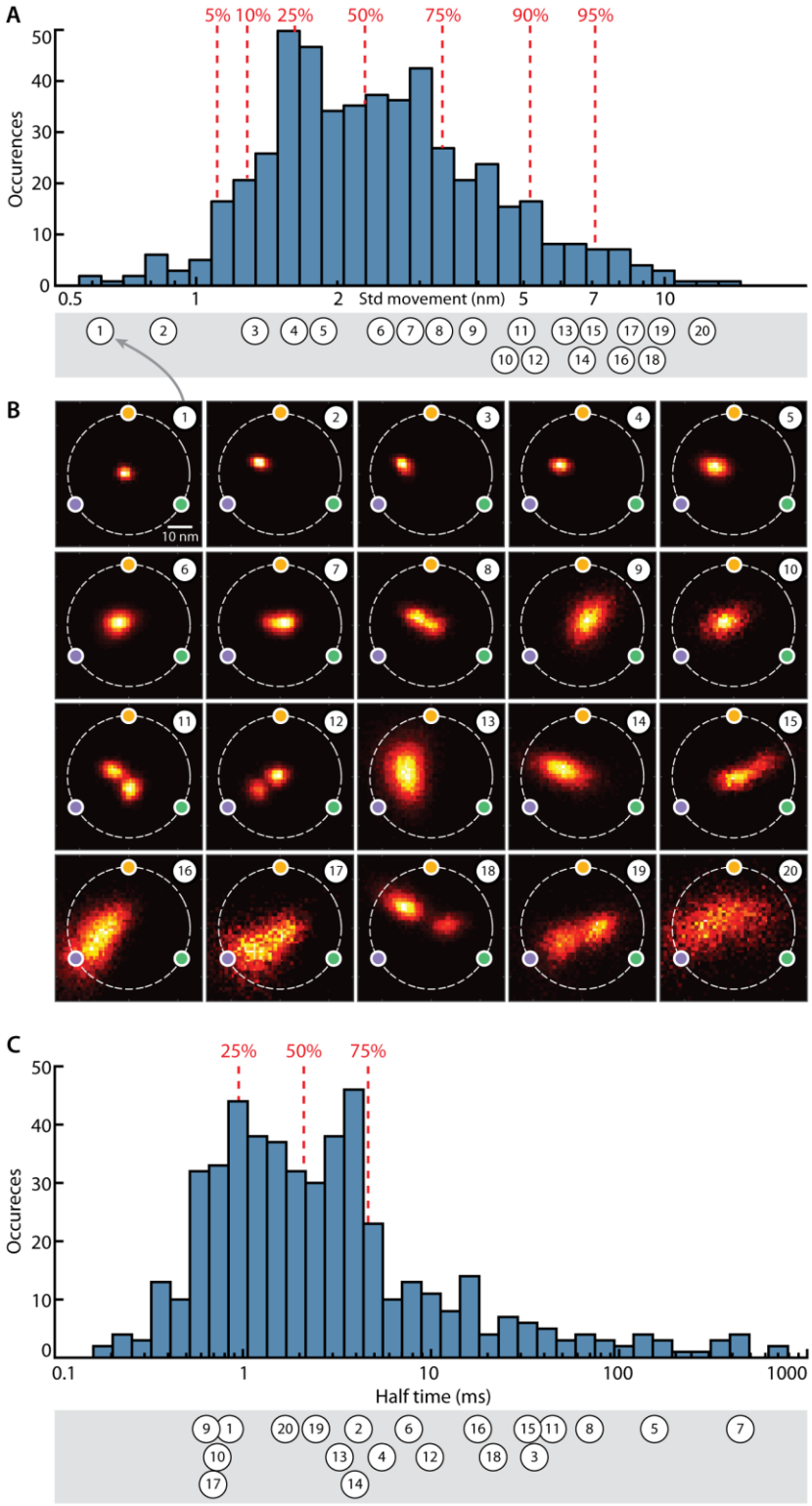

Fig. S4. Classification of recorded emitter movement. (**A**) Occurrences of the standard deviation of the emitter dynamics along the principal axis of the movement σ_{mov}. Additionally, the cumulative sum of the occurrences is shown as red percentage (median 2.3 nm). The majority of the 496 evaluated traces are characterized by either standing still or by moving only slightly. A minority (< 5 %) showed a one-dimensional movement with a peak-to-peak magnitude as expected from sample design. (**B**) Localization histogram of some exemplary traces that span the complete range of the obtained σ_{mov} values. The photon counts and the resulting MINFLUX localizations as well as the autocorrelation analysis that correspond to these traces are visualized in fig. **S5** and **S6**. Note that trace number 19 was discussed in detail in the main text (*Nanometer-scale MINFLUX tracking*). The position of the central doughnut exposure was omitted in all histograms. (**C**) Occurrences of the half-time for correlation of position along the direction of maximal movement (e_2 in fig. 3B). The cumulative sum of the occurrences is shown as red percentage (median 2.1 ms).

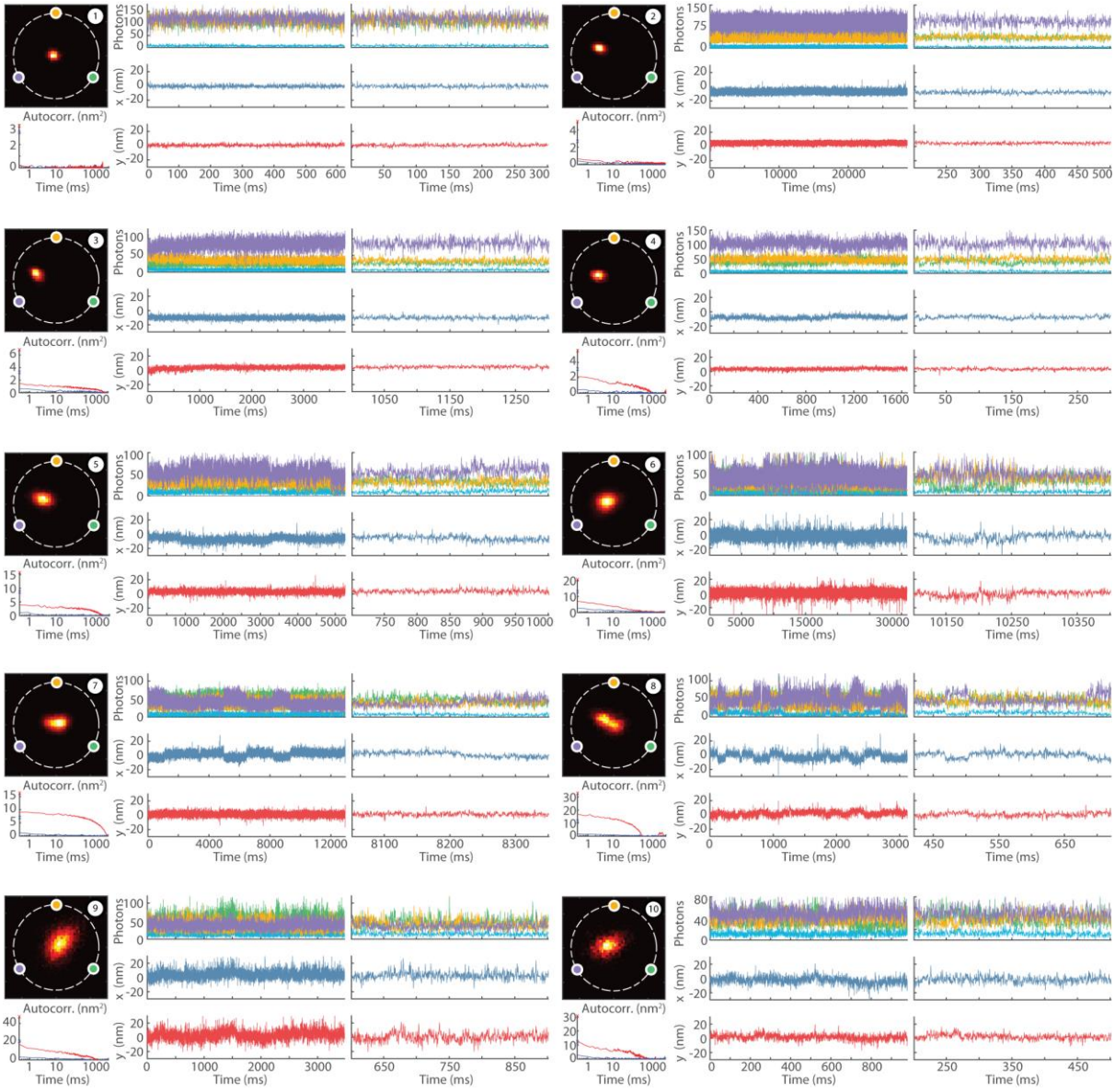

Fig. S5. Details of the localization histograms shown in fig. **S4**. In addition to the photon counts and the MINFLUX localizations of the whole trace a 300 ms trace extract is visualized. Furthermore, the results of the autocorrelation analysis as obtained from the localization trace are shown (see SI Appendix, Autocorrelation analysis).

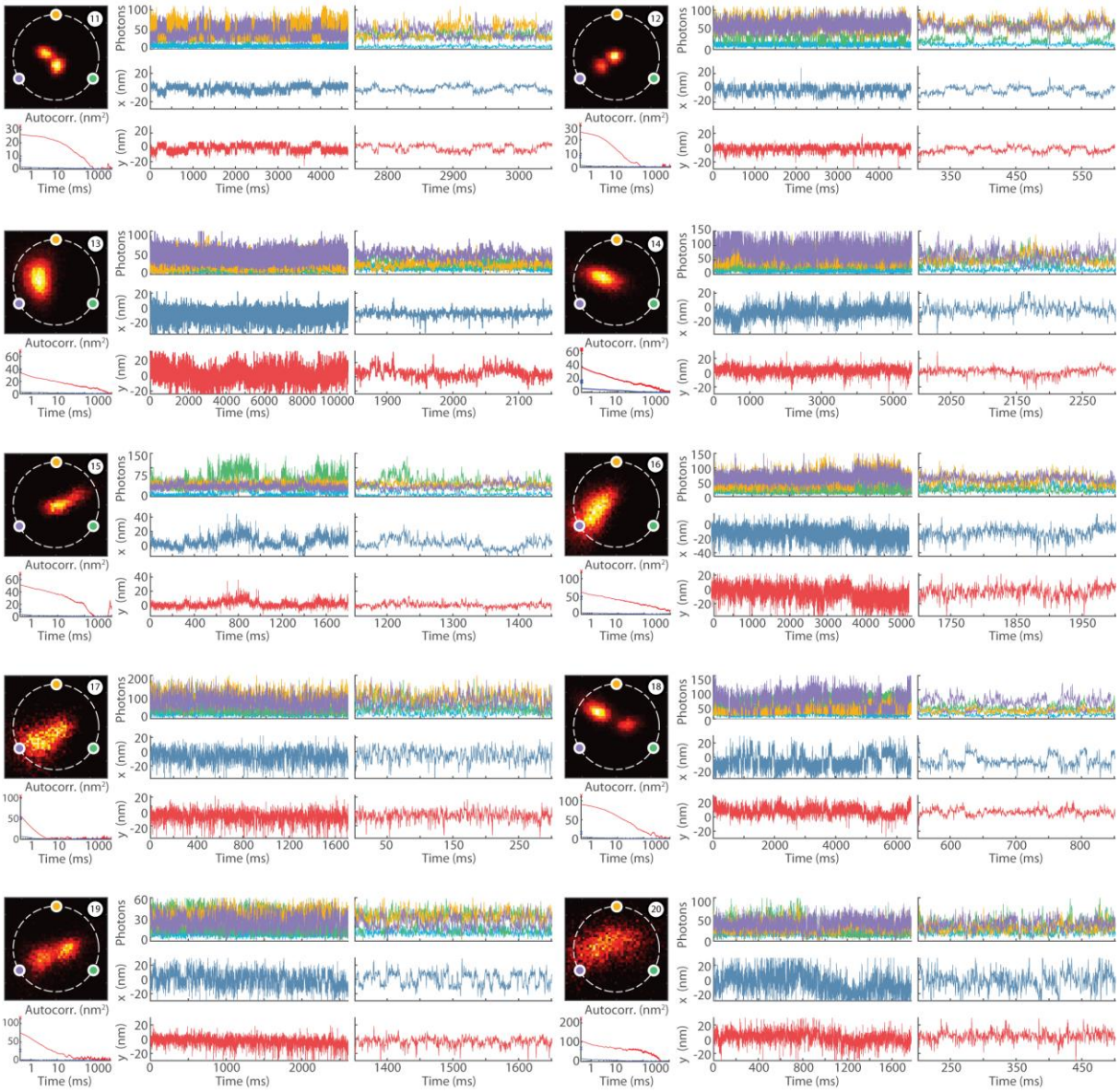

Fig. S6. Details of the localization histograms shown in fig. **S4**. In addition to the photon counts and the MINFLUX localizations of the whole trace, a 300 ms trace extract is visualized. Furthermore, the results of the autocorrelation analysis as obtained from the localization trace are shown (see SI Appendix, Autocorrelation analysis).

Blinking kinetics

An intrinsic assumption made in MINFLUX localization is the linearity of the mean fluorescence signal λ_i obtained from an exposure to the excitation intensity $I_i(\bar{r}_m)$ (eq. (S1)). Should the emitter be in a fluorescence off-state during one of the exposures in a multiplex cycle, the resulting count vector is no longer indicative of the true emitter position. It is thus important to measure the characteristic blinking kinetics. To estimate the emitter off time τ_{off} the photon arrival times were measured for an ensemble of 20 ATTO 647N molecules. A $50{:}\,50$ beam splitter randomly distributed the fluorescence photons on two avalanche photo diode (APD) detectors. The temporal correlation function $G^2(\tau)$ of these two time traces was obtained and fitted to the following model (6)

$$G^2(\tau) = G^2(0)\left(1 + \frac{F}{1-F}e^{-\frac{\tau}{\tau_{off}}}\right) + G^2(\infty) \tag{S9}$$

with F being the fraction of the emitter in the fluorescent off state (fig. **S7**A).

The ensemble average was estimated to $\bar{\tau}_{off} = (5.7 \pm 1.4)$ µs (fig. **S7**B), which is on the order of the excitation gate of 17 µs (fig. **S2**). To reduce the deteriorating effect of the blinking, one can bin the obtained counts of an exposure across different multiplex cycles (SI Appendix, Segmentation and binning of the count traces). In this study, typically four cycles were binned yielding effective photon collection times of 68 µs per doughnut exposure, yielding effective photon collection times that are an order of magnitude larger than τ_{off}. The resulting time resolution of the binned photon collection, and therefore of one MINFLUX localization, is 400 µs in this case.

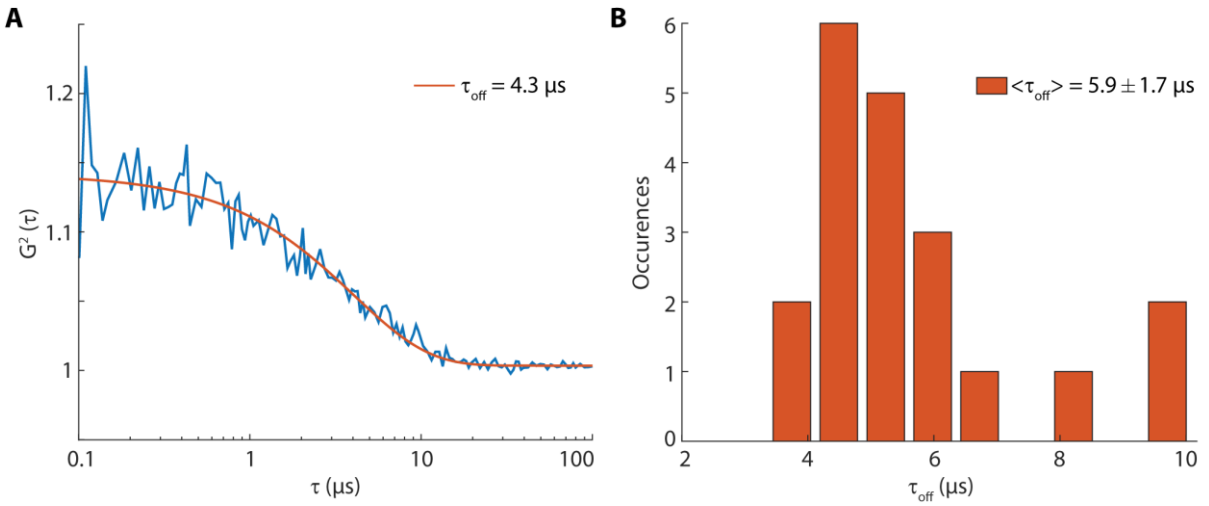

Fig. S7. Blinking kinetics of ATTO 647N. (**A**) Temporal correlation function of the photon arrival times of an ATTO 647N emitter. The emitter blinking off time τ_{off} was estimated to $\tau_{off} = 4.3$ µs by a fit to a model (eq. (S9)). (**B**) Measurement of 20 different ATTO 647N emitters yields an average blinking off time of $\langle\tau_{off}\rangle = 5.9 \pm 1.7$ µs.

Cramér-Rao bound

The Cramér-Rao bound (CRB) is a concept from estimation theory which describes the best possible precision with which a parameter of interest can be estimated. Here, the parameter of interest is the molecule position. The lower bound on the covariance matrix $\Sigma(\bar{r})$ thus given by the CRB $\Sigma_{\mathrm{CRB}}(\bar{r})$

$$\Sigma(\bar{\mathrm{r}}) \geq \Sigma_{\mathrm{CRB}}(\bar{r}) \tag{S10}$$

For the multinomial distribution $P(\bar{n}|N,\bar{r})$, the CRB was derived previously (4) and is given by

$$\begin{aligned}\Sigma_{CRB}(\bar{r}) = \frac{1}{N}\left(\left[\sum_{i=0}^{K-1}\frac{1}{p_i}\left(\frac{\partial p_i}{\partial x}\right)^2\right]\left[\sum_{i=0}^{K-1}\frac{1}{p_i}\left(\frac{\partial p_i}{\partial y}\right)^2\right]-\left[\sum_{i=0}^{K-1}\frac{1}{p_i}\frac{\partial p_i}{\partial x}\frac{\partial p_i}{\partial y}\right]^2\right)^{-1}\\ \times\sum_{i=0}^{K-1}\frac{1}{p_i}\begin{bmatrix}\left(\frac{\partial p_i}{\partial y}\right)^2 & -\frac{\partial p_i}{\partial x}\frac{\partial p_i}{\partial y}\\ -\frac{\partial p_i}{\partial x}\frac{\partial p_i}{\partial y} & \left(\frac{\partial p_i}{\partial x}\right)^2\end{bmatrix}\end{aligned} \tag{S11}$$

The arithmetic mean of its eigenvalues follows from eq. (S4)

$$\sigma_{CRB} = \frac{1}{\sqrt{N}}\sqrt{\frac{\sum_{i=0}^{K-1}\frac{1}{p_i}\left[\left(\frac{\partial p_i}{\partial y}\right)^2+\left(\frac{\partial p_i}{\partial x}\right)^2\right]}{2\left[\sum_{i=0}^{K-1}\frac{1}{p_i}\left(\frac{\partial p_i}{\partial x}\right)^2\right]\left[\sum_{i=0}^{K-1}\frac{1}{p_i}\left(\frac{\partial p_i}{\partial y}\right)^2\right]-\left[\sum_{i=0}^{K-1}\frac{1}{p_i}\frac{\partial p_i}{\partial x}\frac{\partial p_i}{\partial y}\right]^2}} \tag{S12}$$

MINFLUX CRB

The MINFLUX CRB visualized in fig. **1**C-E assumed the following doughnut shaped intensity profile

$$\mathrm{I}_{\mathrm{doughnut}}(\bar{r}) = A_0\frac{r^2}{fwhm^2}e^{\frac{-4\log(2)r^2}{fwhm^2}} \tag{S13}$$

The corresponding probability vector $\bar{p}(\bar{r})$ is obtained by inserting eq. (S13) into eq. (S1). Inserting the probability vector $\bar{p}(\bar{r})$ into eq. (S11) for $K = 4$ exposures yields the lower bound on the covariance matrix $\Sigma_{CRB}(\bar{r})$ and insertion into eq. (S12) the bound σ_{CRB} on the localization precision. A cross section of $\sigma_{CRB}(\bar{r})$ for different L-values without and with background contributions is shown (fig. **S8**).

The lower bound on the localization precision σ_{CRB} visualized in fig. **2**D was calculated from the experimentally measured excitation profile. Thereby, the probability vector $\bar{p}(\bar{r})$ was obtained as explained (SI Appendix, Localization precision). In all cases, the evaluation was done numerically in MATLAB.

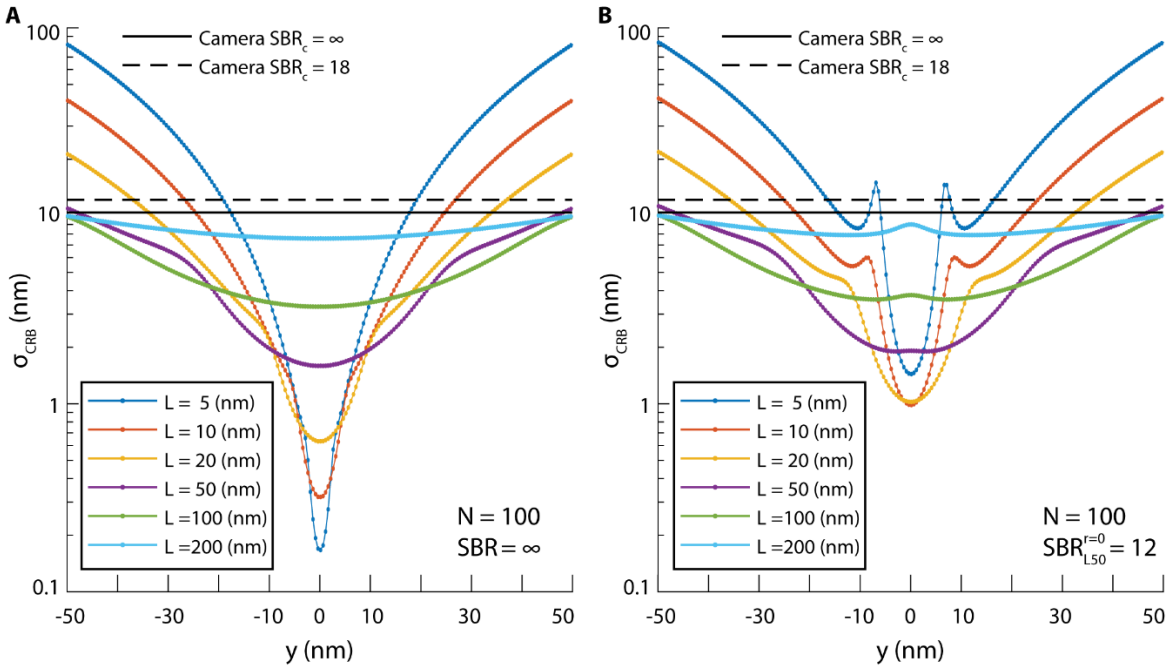

Fig. S8. MINFLUX Cramér-Rao bound $\sigma_{CRB}(\bar{r})$ for the excitation beam pattern shown in fig. **1**B along the y-axis for different beam separation L-values. (**A**) $\mathrm{SBR} = \infty$, total number of photons $N = 100$. Highest localization precision is found around the STC center and deteriorates with increasing distance to it. Lower L-values grant higher localization precision, however, they confine it to a small region. (**B**) $\mathrm{SBR}^{r=0}_{L=50} = 12$ ($SBR = 12$ at $\bar{r} = \bar{0}$ for $L = 50$ nm), total number of photons $N = 100$. The localization precision in the vicinity of the origin improves only up to a given L-value due to background.

Camera CRB

The camera CRB was calculated as described previously (4). In brief, the emitter photons reaching the detector were assumed to follow Poissonian statistics with parameter λ_{tot} and to generate a Gaussian shaped PSF

$$I_{Gauss}(x,y) = A_{gauss} e^{-\frac{1}{2}\left(\frac{x-x_m}{\sigma_{PSF}}\right)^2} e^{-\frac{1}{2}\left(\frac{y-y_m}{\sigma_{PSF}}\right)^2} \tag{S14}$$

Effects of pixelation and Poissonian noise contributions with parameter λ_b were taken into account. The following results can be understood as a lower bound on the camera performance given that further noise sources like read noise or excess noise were neglected.

The probability $p_i(\bar{r}_m)$ to detect a photon in pixel i given an emitter at position $\bar{r}_m$ can be written as

$$\begin{aligned} p_i(x_m, y_m) = {} & \frac{\xi}{\xi \cdot K + SBR_c} + \frac{SBR_c}{\xi \cdot K + SBR_c} \cdot \frac{1}{4} \\ & \cdot \left(\mathrm{erf}\left(\frac{x_i + a/2 - x_m}{\sqrt{2}\,\sigma_{PSF}} \right) - \mathrm{erf}\left(\frac{x_i - a/2 - x_m}{\sqrt{2}\,\sigma_{PSF}} \right) \right) \\ & \cdot \left(\mathrm{erf}\left(\frac{y_i + a/2 - y_m}{\sqrt{2}\,\sigma_{PSF}} \right) - \mathrm{erf}\left(\frac{y_i - a/2 - y_m}{\sqrt{2}\,\sigma_{PSF}} \right) \right) \end{aligned} \tag{S15}$$

where a is the pixel size with its center at $[x_i, y_i]$ and K the number of pixel considered. Typically, $K = 9 \times 9$ pixel were used with a size of $a = 100$ nm, respectively. The parameter $\xi = a^2/\pi(3\sigma_{PSF})^2$ describes the ratio of the area of a pixel to the area of the Gaussian shaped PSF that containing about 99% of the fluorescence photons ($a_{99} = \pi(3\sigma_{PSF})^2$).

The camera signal to background ratio (SBR_c) is defined as

$$SBR_c = \frac{\lambda_{tot}}{\lambda_b} \tag{S16}$$

where λ_b is the mean background signal in a_{99}. Note the different SBR_c definition compared to (4). In the definition used in that article, a signal to background ratio of 500 corresponds to $SBR_c \approx 17.5$ in the new definition. The camera CRB is obtained by inserting eq. (S15) into (S12).

Captions for supplementary movies

Movie S1. Trajectory of the 1D bridge diffuser (green diamond) from fig. 3 slowed down 25 times, at a time resolution of 1ms. As time advances, a histogram of the emitter locations is constructed.

Movie S2. Trajectory of the 1D bridge diffuser (green diamond) from fig. 3 slowed down 100 times, at a time resolution of 400µs. As time advances, a histogram of the emitter locations is constructed.

Staples and DNA strand sequences

Origami staples			
#	Sequence		
2	ACGTTAGTAAATGAATTTTCTGTAAGCGGAGT	110	GCTAAATCCTGTAGCTCAACATGTATTGCTGA
3	CGTAACGATCTAAAGTTTTGTCGTGAATTGCG	111	CAAAATTAAAGTACGGTGTCTGGAAGAGGTCA
4	TGTAGCATTCCACAGACAGCCCTCATCTCCAA	112	CAATAAATACAGTTGATTCCCAATTTAGAGAG
5	TGAGTTTCGTCACCAGTACAAACTTAATTGTA	113	TCAATTCTTTTAGTTTGACCATTACCAGACCG
6	CAAGCCCAATAGGAACCCATGTACCGTAACAC	114	TTTCATTTGGTCAATAACCTGTTTAATCAATA
7	CTCAGAGCCACCACCCTCATTTTCCTATTATT	115	CTAATTTATCTTTCCTTATCATTCATCCTGAA
8	CCCTCAGAACCGCCACCCTCAGAACTGAGACT	116	TAAGTCCTACCAAGTACCGCACTCTTAGTTGC
9	TATCACCGTACTCAGGAGGTTTAGCGGGGTTT	117	AATGCAGACCGTTTTTATTTTCATCTTGCGGG
12	AATAATAAGGTCGCTGAGGCTTGCAAAGACTT	118	CCAGACGAGCGCCCAATAGCAAGCAAGAACGC
13	AAAAAAGGACAACCATCGCCCACGCGGGTAAA	119	CTGTAATATTGCCTGAGAGTCTGGAAAACTAG
14	TCGGTTTAGCTTGATACCGATAGTCCAACCTA	120	CAACGCAATTTTTGAGAGATCTACTGATAATC
15	AATGCCCCGTAACAGTGCCCGTATGTGAATTT	121	TATATTTTAGCTGATAAATTAATGTTGTATAA
16	CTGAAACAGGTAATAAGTTTTAACCCCTCAGA	122	AGGTAAAGAAATCACCATCAATATAATATTTT
17	CCTCAAGAATACATGGCTTTTGATAGAACCAC	124	ACGCTCAAAATAAGAATAAACACCGTGAATTT
18	TGCTCAGTCAGTCTCTGAATTTACCAGGAGGT	125	CATATTTAGAAATACCGACCGTGTTACCTTTT
21	AAAGGCCGAAAGGAACAACTAAAGCTTTCCAG	126	AGAGGCATAATTTCATCTTCTGACTATAACTA
22	ATATATTCTTTTTTCACGTTGAAAATAGTTAG	129	TCAGGTCACTTTTGCGGGAGAAGCAGAATTAG
23	CAATGACACTCCAAAAGGAGCCTTACAACGCC	130	GGTAGCTAGGATAAAAATTTTTAGTTAACATC
24	CTTAAACATCAGCTTGCTTTCGAGAAACAGTT	131	ACCGTTCTAAATGCAATGCCTGAGAGGTGGCA
25	TGCCTTGACTGCCTATTTCGGAACAGGGATAG	132	AGACAGTCATTCAAAAGGGTGAGATATCATAT
26	AGTGTACTTGAAAGTATTAAGAGGCCGCCACC	133	AATTACTACAAATTCTTACCAGTAATCCCATC
27	TAAGCGTCGAAGGATTAGGATTAGTACCGCCA	134	AGGCGTTACAGTAGGGCTTAATTGACAATAGA
29	ACGGCTACTTACTTAGCCGGAACGCTGACCAA	135	AATGGTTTACAACGCCAACATGTAGTTCAGCT
30	TTTCATGAAAATTGTGTCGAAATCTGTACAGA	136	TTTTAGTTTTTCGAGCCAGTAATAAATTCTGT
31	ATACGTAAAAGTACAACGGAGATTTCATCAAG	137	CATGTCAAGATTCTCCGTGGGAACCGTTGGTG
32	AAACGAAATGACCCCCAGCGATTATTCATTAC	138	AGAAAAGCAACATTAAATGTGAGCATCTGCCA
33	GAGCCGCCCCACCACCGGAACCGCCTAAAACA	139	GCAAATATCGCGTCTGGCCTTCCTGGCCTCAG
34	GCCACCACTCTTTTCATAATCAAACCGTCACC	140	GTTAAAATTTTAACCAATAGGAACCCGGCACC
35	CACCAGAGTTCGGTCATAGCCCCCGCCAGCAA	141	TTAAGACGTTGAAAACATAGCGATTTAAATCA
36	TGAGGCAGGCGTCAGACTGTAGCGTAGCAAGG	142	ATCAAAATCGTCGCTATTAATTAACGGATTCG
39	GCTCCATGAGAGGCTTTGAGGACTAGGGAGTT	143	TAACCTCCATATGTGAGTGAATAAACAAAATC
40	CGCCTGATGGAAGTTTCCATTAAACATAACCG	144	TATGTAAACCTTTTTTAATGGAAAAATTACCT
41	GCGAAACATGCCACTACGAAGGCATGCGCCGA	147	ACCCGTCGTCATATGTACCCCGGTAAAGGCTA
42	CTCATCTTGAGGCAAAAGAATACACTCCCTCA	148	CTTTCATCCCCAAAAACAGGAAGACCGGAGAG
43	AACCAGAGACCCTCAGAACCGCCAGGGGTCAG	149	AAATAATTTTAAATTGTAAACGTTGATATTCA
44	GTTTGCCACCTCAGAGCCGCCACCGATACAGG	150	GCTCATTTTCGCATTAAATTTTTGAGCTTAGA
45	TCGGCATTCCGCCGCCAGCATTGACGTTCCAG	151	TAGAATCCCTGAGAAGAGTCAATAGGAATCAT
46	TGCCTTTAGTCAGACGATTGGCCTGCCAGAAT	152	CTGTAAATCATAGGTCTGAGAGACGATAAATA
47	CTTTGAAAAGAACTGGCTCATTATTTAATAAA	153	AAATCAATGGCTTAGGTTGGGTTACTAAATTT
48	CCAGGCGCTTAATCATTGTGAATTACAGGTAG	154	TTGAATTATGCTGATGCAAATCCACAAATATA
49	AGTAATCTTAAATTGGGCTTGAGAGAATACCA	155	TAGATGGGGGGTAACGCCAGGGTTGTGCCAAG
50	CCAAATCACTTGCCCTGACGAGAACGCCAAAA	156	GTTTGAGGGAAAGGGGGATGTGCTAGAGGATC
51	TTATTCATAGGGAAGGTAAATATTCATTCAGT	157	GAAGATCGGTGCGGGCCTCTTCGCAATCATGG
52	GACTTGAGAGACAAAAGGGCGACAAGTTACCA	158	GCTTCTGGTCAGGCTGCGCAACTGTGTTATCC
53	AATCACCAAATAGAAAATTCATATATAACGGA	159	CTTTTACACAGATGAATATACAGTAAGCGCCA
54	CCGGAAACACACCACGGAATAAGTAAGACTCC	160	CCTGATTGAAAGAAATTGCGTAGACCCGAACG
57	CGATTTTAGAGGACAGATGAACGGCGCGACCT	161	GCGCAGAGATATCAAAATTATTTGACATTATC
58	TTTCAACTATAGGCTGGCTGACCTTGTATCAT	162	GAGCAAAAACTTCTGAATAATGGAAGAAGGAG
59	ACGAGTAGTGACAAGAACCGGATATACCAAGC	165	ATTAAGTTCGCATCGTAACCGTGCGAGTAACA
60	GAATAAGGACGTAACAAAGCTGCTGACGGAAA	166	CAGCTGGCGGACGACGACAGTATCGTAGCCAG
61	ATTGAGGGTAAAGGTGAATTATCAATCACCGG	167	GGCGATCGCACTCCAGCCAGCTTTGCCATCAA
62	AGCGCCAACCATTTGGGAATTAGATTATTAGC	168	TTCGCCATTGCCGGAAACCAGGCAAACAGTAC
63	TCACAATCGTAGCACCATTACCATCGTTTTCA	169	TTTAACGTTCGGGAGAAACAATAATTTTCCCT
64	ACGCAAAGGTCACCAATGAAACCAATCAAGTT	170	ACAGAAATCTTTGAATACCAAGTTCCTTGCTT

65	ACGAACTAGCGTCCAATACTGCGGAATGCTTT	171	AACCTACCGCGAATTATTCATTTCCAGTACAT
66	AAAGATTCAGGGGGTAATAGTAAACCATAAAT	172	TGGATTATGAAGATGATGAAACAAAATTTCAT
67	CATTCAACGCGAGAGGCTTTTGCATATTATAG	173	CTTGCATGCATTAATGAATCGGCCCGCCAGGG
68	GGAATTACTCGTTTACCAGACGACAAAAGATT	174	CCCGGGTACTTTCCAGTCGGGAAACGGGCAAC
69	AAAAGTAATATCTTACCGAAGCCCAACACTAT	175	TCATAGCTACTCACATTAATTGCGCCCTGAGA
70	GAAGGAAAATAAGAGCAAGAAACAACAGCCAT	176	GCTCACAATGTAAAGCCTGGGGTGGGTTTGCC
71	ATACCCAAGATAACCCACAAGAATAAACGATT	177	CGACAACTAAGTATTAGACTTTACAGCCGGAA
72	TTATTACGGTCAGAGGGTAATTGAATAGCAGC	178	TTATTAATGCCGTCAATAGATAATCAGAGGTG
75	ACTGGATAACGGAACAACATTATTACCTTATG	179	ATTTTGCGTCTTTAGGAGCACTAAGCAACAGT
76	TTTGCCAGATCAGTTGAGATTTAGTGGTTTAA	180	CGGAATTATTGAAAGGAATTGAGGTGAAAAAT
77	CCAAAATATAATGCAGATACATAAACACCAGA	183	GCCAGCTGCCTGCAGGTCGACTCTGCAAGGCG
78	CATAACCCGAGGCATAGTAAGAGCTTTTTAAG	184	ACTGCCCGCCGAGCTCGAATTCGTTATTACGC
79	GCAATAGCGCAGATAGCCGAACAATTCAACCG	185	GTGAGCTAGTTTCCTGTGTGAAATTTGGGAAG
80	GCCCAATACCGAGGAAACGCAATAGGTTTACC	186	GCATAAAGTTCCACACAACATACGAAACAATT
81	ATCAGAGAAAGAACTGGCATGATTTTATTTTG	187	GGATTTAGCGTATTAAATCCTTTGTTTTCAGG
82	TGAACAAACAGTATGTTAGCAAACTAAAAGAA	188	AGATTAGATTTAAAAGTTTGAGTACACGTAAA
83	AAACAGTTGATGGCTTAGAGCTTATTTAAATA	189	CTAAAATAGAACAAAGAAACCACCAGGGTTAG
84	CAAAAATCATTGCTCCTTTTGATAAGTTTCAT	190	ATCAACAGTCATCATATTCCTGATTGATTGTT
85	TCAGAAGCCTCCAACAGGTCAGGATCTGCGAA	192	AGCTGATTACAAGAGTCCACTATTGAGGTGCC
86	AAGAGGAACGAGCTTCAAAGCGAAGATACATT	193	GAGTTGCACGAGATAGGGTTGAGTAAGGGAGC
87	CCTAATTTACGCTAACGAGCGTCTATATCGCG	194	CCAGCAGGGGCAAAATCCCTTATAAAGCCGGC
88	ATTATTTAACCCAGCTACAATTTTCAAGAACG	195	ACGAACCAAAACATCGCCATTAAATGGTGGTT
89	TTTTGTTTAAGCCTTAAATCAAGAATCGAGAA	196	AGGCGGTCATTAGTCTTTAATGCGCAATATTA
90	CTTTACAGTTAGCGAACCTCCCGACGTAGGAA	197	GCCACGCTATACGTGGCACAGACAACGCTCAT
93	TTTTTGCGCAGAAAACGAGAATGAATGTTTAG	198	CTAAAGCAAGATAGAACCCTTCTGAATCGTCT
94	TACCTTTAAGGTCTTTACCCTGACAAAGAAGT	201	TGGACTCCCTTTTCACCAGTGAGACCTGTCGT
95	GAAGCAAAAAAGCGGATTGCATCAGATAAAAA	202	AGTTTGGAGCCCTTCACCGCCTGGTTGCGCTC
96	TTTTAATTGCCCGAAAGACTTCAATTCCAGAG	203	GAATAGCCGCAAGCGGTCCACGCTCCTAATGA
97	TCTTACCAGCCAGTTACAAAATAAATGAAATA	204	CCGAAATCCGAAAATCCTGTTTGAAATACCGA
98	TATTTTGCTCCCAATCCAAATAAGTGAGTTAA	205	TAGCCCTACCAGCAGAAGATAAAAACATTTGA
99	AGGTTTTGAACGTCAAAAATGAAAGCGCTAAT	206	GAATGGCTAGTATTAACACCGCCTCAACTAAT
100	GAGGCGTTAGAGAATAACATAAAAGAACACCC	207	GCGTAAGAGAGAGCCAGCAGCAAAAAGGTTAT
101	TGCAACTAAGCAATAAAGCCTCAGTTATGACC	210	ACCCAAATCAAGTTTTTTGGGGTCAAAGAACG
102	TCCATATACATACAGGCAAGGCAACTTTATTT	211	GTAAAGCACTAAATCGGAACCCTAGTTGTTCC
103	CGAGTAGAACTAATAGTAGTAGCAAACCCTCA	212	CCCCGATTTAGAGCTTGACGGGGAAATCAAAA
104	TCGCAAATGGGGCGCGAGCTGAAATAATGTGT	213	GAACGTGGCGAGAAAGGAAGGGAACAAACTAT
105	ATCGGCTGCGAGCATGTAGAAACCAGCTATAT	214	CGGCCTTGCTGGTAATATCCAGAACGAACTGA
106	GGTATTAAGAACAAGAAAAATAATTAAAGCCA	215	CCGCCAGCCATTGCAACAGGAAAAATATTTTT
107	CAAGCAAGACGCGCCTGTTTATCAAGAATCGC	216	GGAAATACCTACATTTTGACGCTCACCTGAAA
108	TCATTACCCGACAATAAACAACATATTTAGGC	217	GAAATGGATTATTTACATTGGCAGACATTCTG
109	TATAGAAGCGACAAAAGGTAAAGTAGAGAATA		

Biotinylated Strands		
5' biotin modification		
#	Sequence	Length (bases)
11	GAGAATAGCTTTTGCGGGATCGTCGGGTAGCA	32
191	TGGTTTTTAACGTCAAAGGGCGAAGAACCATC	32
123	GCGTTATAGAAAAAGCCTGTTTAGAAGGCCGG	32
28	GGAAAGCGACCAGGCGGATAAGTGAATAGGTG	32
208	GCCAACAGTCACCTTGCTGAACCTGTTGGCAA	32
76 single molecule helper	TTA TTC CTG TAG TAT ATG GCA ATG AAA TTA T --	
	TTTGCCAGATCAGTTGAGATTTAGTGGTTTAA	
Single molecule strand		Positition
SM strand	TAA **T**TT CAT TGC CAT ATA CTA CAG GAA TAA	4: ATTO647N
Nes22 & Nes76 helper		
1DD 22	AATGGGGAAGAGGGCGTTACCTGCAAGTCTAATTGCC --	
	AATACC ATATATTCTTTTTTCACGTTGAAAATAGTTAG	
1DD 76	TTTGCCAGATCAGTTGAGATTTAGTGGTTTAA TGGATA --	
	GAGGCTATGAGATTGTCTCCAGCAAGCAAGCCATATT	
Bridge		Position
1DD bridge	GTATTGGCAATTAGACTTGCAGGTAACGCCCTCTTCCCCAT --	
	T**T**AATATGGCTTGCTTGCTGGAGACAATCTCATAGCCTCTATCC	43: ATTO647N

References

1. Rothemund PW (2006) Folding DNA to create nanoscale shapes and patterns. *Nature* 440(7082):297-302.
2. Brunet A*, et al.* (2015) Dependence of DNA Persistence Length on Ionic Strength of Solutions with Monovalent and Divalent Salts: A Joint Theory-Experiment Study. *Macromolecules* 48(11):3641-3652.
3. Le TT & Kim HD (2014) Probing the elastic limit of DNA bending. *Nucleic Acids Res* 42(16):10786-U10807.
4. Balzarotti F*, et al.* (2017) Nanometer resolution imaging and tracking of fluorescent molecules with minimal photon fluxes. *Science* 355(6325):606-612.
5. Vogelsang J*, et al.* (2008) A Reducing and Oxidizing System Minimizes Photobleaching and Blinking of Fluorescent Dyes. *Angewandte Chemie (international Edition)* 47(29):5465-5469.
6. Widengren J, Mets U, & Rigler R (1995) Fluorescence correlation spectroscopy of triplet-states in solution - a theoretical and experimental-study. *J Phys Chem* 99:13368-13379.